molecular pharmaceutics

Article

pubs.acs.org/molecularpharmaceutics

Investigating Albendazole Desmotropes by Solid-State NMR Spectroscopy

Ana K. Chattah,*[,†] Rongchun Zhang,[‡] Kamal H. Mroue,[‡] Laura Y. Pfund,[§] Marcela R. Longhi,[∥] Ayyalusamy Ramamoorthy,[‡] and Claudia Garnero*[,∥]

[†]Facultad de Matemática, Astronomía y Física and IFEG (CONICET), Universidad Nacional de Córdoba, Ciudad Universitaria, X5000HUA Córdoba, Argentina

[‡]Biophysics and Department of Chemistry, University of Michigan, Ann Arbor, Michigan 48109-1055, United States

[§]Department of Chemistry and the Macromolecular Science and Engineering Program, University of Michigan, Ann Arbor, Michigan 48109-1055, United States

[∥]Departamento de Farmacia, Facultad de Ciencias Químicas and UNITEFA (CONICET), Universidad Nacional de Córdoba, Ciudad Universitaria, X5000HUA Córdoba, Argentina

Supporting Information

ABSTRACT: Characterization of the molecular structure and physicochemical solid-state properties of the solid forms of pharmaceutical compounds is a key requirement for successful commercialization as potential active ingredients in drug products. These properties can ultimately have a critical effect on the solubility and bioavailability of the final drug product. Here, the desmotropy of Albendazole forms I and II was investigated at the atomic level. Ultrafast magic angle spinning (MAS) solid-state nuclear magnetic resonance (NMR) spectroscopy, together with powder X-ray diffraction, thermal analysis, and Fourier transform infrared spectroscopy, were performed on polycrystalline samples of the two solids in order to fully characterize and distinguish the two forms. High-resolution one-dimensional ^{1}H, ^{13}C, and ^{15}N together with two-dimensional $^{1}H/^{1}H$ single quantum−single quantum, $^{1}H/^{1}H$ single quantum−double quantum, and $^{1}H/^{13}C$ chemical shift correlation solid-state NMR experiments under MAS conditions were extensively used to decipher the intramolecular and intermolecular hydrogen bonding interactions present in both solid forms. These experiments enabled the unequivocal identification of the tautomers of each desmotrope. Our results also revealed that both solid forms may be described as dimeric structures, with different intermolecular hydrogen bonds connecting the tautomers in each dimer.

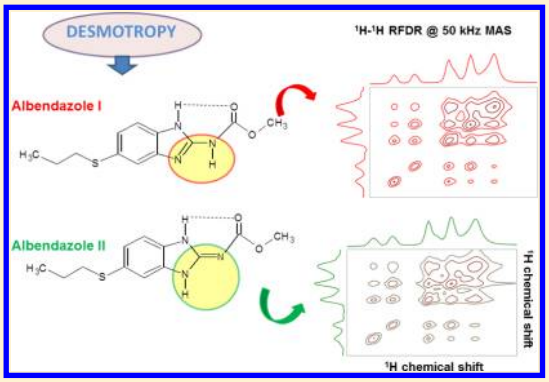

KEYWORDS: *albendazole, desmotropy, tautomerism, solid-state NMR, characterization, ultrafast MAS, RFDR*

1. INTRODUCTION

Desmotropy is a rare phenomenon related to tautomerism, in which both tautomeric forms can been isolated in the solid state. Only few examples are published, most of them concerning heterocycles.[1,2] The term "desmotropes" is not widely known or used within the crystallographic community. However, desmotropy is a different phenomenon than polymorphism (the same tautomer crystallizing in two or more crystal forms) or tautomeric polymorphism.

It is well-known that different solid forms of an active pharmaceutical ingredient (API) may exhibit drastically different physical properties, chemical stability and solubility, which in turn affect their pharmaceutical performance through bioavailability and dissolution behavior.[1] Central to this is the physical form of a drug substance that plays a key role in various stages of the manufacturing process such as grinding, mixing, tablet presentation, etc. Therefore, a comprehensive solid-state characterization of an API is crucial to numerous entities involved in pharmaceutical development.[2]

Albendazole (ABZ), methyl[5-(propylthio)-1*H*-benzimidazol-2yl] carbamate (Scheme 1), is a benzimidazole derivative with a broad-spectrum of activity against human and animal helminthes parasites.[3,4] Parasitic helminthic infections are an important cause of morbidity and mortality worldwide. ABZ, an API present in the World Health Organization (WHO) list of essential medicines,[5] is effective in the control and treatment of parasitic infections (such as echinococcosis, hydatidosis, and neurocysticercosis) and may have a potential role in lymphatic filariasis control.[6] Due to its relatively low cost, good tolerance, and broad-spectrum of activity, ABZ is one of the most

Received: August 7, 2014
Revised: December 11, 2014
Accepted: January 13, 2015

DOI: 10.1021/mp500539g
Mol. Pharmaceutics XXXX, XXX, XXX−XXX

Scheme 1. ABZ Tautomers Corresponding to Desmotropic Forms I (a) and II (b)

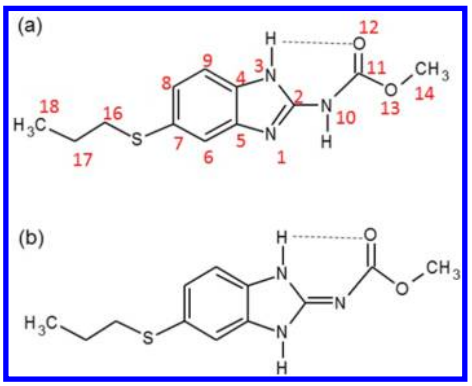

commercialized benzimidazole derivatives in the world and is considered the drug of choice for helminthic intestinal infections in tropical and subtropical countries.[7] However, ABZ suffers from low and erratic oral bioavailability caused by poor solubility and slow dissolution rate in aqueous media. It has been reported that the poor aqueous solubility of the benzimidazole carbamates is most likely due to the presence of intramolecular hydrogen bonds in these compounds.[8]

A recent report that focuses on the polymorphic nature of ABZ describes the existence of two different solid forms (designated by I and II) that are enantiotropically related, giving the single crystal structure information for form II.[9] Moreover, a tautomeric process has been described recently for the molecular arrangements in benzimidazole carbamate derivatives,[10] which involves the two nitrogen atoms present in the five-membered ring and the nitrogen in the carbamate moiety. As tautomeric forms of a molecule exhibit different functional groups, it is expected that this phenomenon affects the binding of the API to the active site of the target. Recently, the role of tautomers has been highlighted as therapeutically significant.[11] The identification of a tautomer in different solid forms of an API is therefore important to evaluate the solid form with improved solubility and bioavailability properties. In this respect, the existing conflict in the assignment of ABZ as a class II or class IV substance in the Biopharmaceutics Classification System[12] makes this API an important case of study.

Solid-state nuclear magnetic resonance (ssNMR) spectroscopy is one of the main techniques to investigate the solid-state molecular structure of an API. In order to obtain high resolution information at the molecular level, it is necessary to utilize ssNMR techniques with fast magic angle spinning (MAS).[13,14] By virtue of the recent technological and instrumental advancements in NMR, high-resolution one-dimensional (1D) and two-dimensional (2D) solid-state NMR techniques, particularly those based on ^{1}H-detection, are gaining considerable popularity nowadays and have recently been applied to a wide variety of systems.[15−19] In particular, the recent introduction of ultrafast MAS NMR probes that can achieve sample spinning rates up to 110 kHz makes it possible to obtain multidimensional high-resolution ^{1}H NMR spectra of organic solids, which facilitates structural and dynamic characterization of pharmaceutical systems at the atomic level.[20−22] A significant body of information can be retrieved from solid-state 1D ^{1}H NMR spectra and 2D ^{1}H/^{1}H single quantum−single quantum (SQ−SQ) experiments utilizing the finite-pulse radiofrequency-driven recoupling sequence (fp-RFDR) for dipolar recoupling under ultrafast MAS[23−27] and single quantum−double quantum (SQ−DQ) experiments.[28−32] The visualization of ^{1}H−^{1}H interactions is particularly useful in small API molecules and pharmaceutical complexes, as it provides unique information on both intramolecular and intermolecular interactions, molecular packing, and hydrogen bonding.[33−35] In addition, the known examples about desmotropy have been investigated mainly with the aid of solid-state NMR and infrared spectroscopy.[36]

The aim of the present study is to characterize and distinguish the two solid forms of ABZ at the atomic level. The solid-state properties of each form were characterized using a combination of classical methods, such as powder X-ray diffraction, thermal analysis, and infrared spectroscopy. Subsequently, particular attention has been given on the identification of each tautomer, as well as on hydrogen bonding and molecular arrangements in the solid-state, from the perspective of high-resolution ssNMR techniques, in particular 1D ^{1}H, ^{13}C, and ^{15}N chemical shift spectra and 2D ^{1}H/^{1}H SQ−SQ fp-RFDR, ^{1}H/^{1}H SQ−DQ, and ^{1}H/^{13}C chemical shift correlation spectra.

2. EXPERIMENTAL SECTION

2.1. Chemicals and Reagents. Albendazole (ABZ) was provided by Todo Droga (Argentina), while BrK and DMSO-d_6 were purchased from Merck (Germany and Switzerland, respectively). Methanol, analytical reagent grade, was purchased from Cicarelli (Argentina).

2.2. Obtaining the Form II of Albendazole. The solid form II of Albendazole was recrystallized from a methanol solution as reported by Pranzo et al.[9] ABZ form I that corresponds to the commercially available ABZ was dissolved in methanol, heated, and stirred until a clear solution was formed. The solution was then filtered, followed by slow evaporation of the solvent under ambient conditions until crystallization was complete. Light brown crystals were collected after 10 days.

2.3. Powder X-ray Diffraction (PXRD). Powder X-ray diffraction patterns were obtained at ambient temperature using a Bruker D8 Advance diffractometer, operating at 40 kV and 40 mA with Cu−Kα radiation (1.5406 Å). All samples were packed into the depression of an indented quartz slide. The powder pattern was collected by scanning 2θ from 3° to 70° with a step size of 0.04° at a scanning rate of 1.5 s/step.

2.4. Differential Scanning Calorimetry (DSC). Thermograms of the samples were recorded on a TA Instruments DSC Q20. Data were analyzed with the TA Universal Analysis software Version 4.3A. Samples (1.0 mg weighed to a precision of 0.0001 mg) were placed on TA Tzero hermetic pans crimped using a TA Tzero press. Thermal behavior of the samples was studied under a nitrogen purge at a heating rate of 10 °C/min, starting at room temperature and ramped to 300 °C. The integrated limits were chosen to encompass all thermal events from initial transformations through melting (200−230 °C) such that the overall enthalpy of melting could be estimated for each form. The melting points refer to the onset of the first endotherm. The instrument was initially calibrated with an indium standard.

2.5. Thermal Gravimetric Analysis (TGA). TGA was recorded on a TA Instruments TGA Q50. Data were analyzed with TA Universal Analysis software Version 4.3A. Thermal behavior of the samples was studied under a nitrogen purge at a heating rate of 10 °C/min over a temperature range of 25−400 °C.

DOI: 10.1021/mp500539g
Mol. Pharmaceutics XXXX, XXX, XXX−XXX

2.6. FT-IR Spectroscopy. The FT-IR spectra were recorded on a Nicolet 5 SXC FT-IR Spectrophotometer (Madison, WI, USA), with the potassium bromide disks being prepared by compressing the powder.

2.7. Solution NMR Spectroscopy. Solution ^{1}H and ^{13}C NMR spectra were acquired for ABZ I and II on a Bruker Avance II High Resolution 400 MHz Spectrometer. The samples were dissolved in DMSO-d_6, and the spectra were recorded at 298 K using a 5 mm sample tube.

2.8. Solid-State NMR Spectroscopy. All ^{1}H MAS NMR experiments were performed on an Agilent VNMRS 600 MHz solid-state NMR spectrometer equipped with a 1.2 mm triple-resonance ultrafast MAS probe, operating on 599.8 MHz frequency for ^{1}H and 150.8 MHz for ^{13}C. All experiments were performed at room temperature. A 90° ^{1}H pulse of 1.2 μs duration was used for single-pulse experiments, while the 90° pulse width was set to 2 μs for the 2D experiments. Single-pulse ^{1}H MAS experiments were performed at MAS rates of 10, 20, 30, 40, 50, and 60 kHz, where it was finally observed that the 50 kHz MAS rate produced spectra with the same proton resolution as those under 60 kHz MAS (see Figure S2 in the Supporting Information). The ^{1}H spin−lattice relaxation (T_1) times under 50 kHz MAS were measured using the inversion−recovery (180°−t−90°−acq) pulse sequence. The recycle delay for all the experiments was set to 12 s. Adamantane was used as external reference for 1D and 2D ^{1}H MAS experiments. All the 1D and 2D spectra in ABZ I and ABZ II were done in the same experimental session and by using the same parameters.

All the ultrafast MAS experiments were performed under 50 kHz MAS condition. $^{1}H/^{1}H$ SQ−SQ fp-RFDR experiments were performed using the pulse sequence described in ref 24, where finite-pulse radio frequency driven recoupling (fp-RFDR) with XY4 phase cycling was utilized during the mixing time for recoupling $^{1}H-^{1}H$ dipolar couplings under 50 kHz MAS (see the pulse sequence given in Figure S1 in the Supporting Information). Two-dimensional $^{1}H/^{1}H$ spectra were obtained using 128 t_1 increments and 48 scans. A series of mixing times between 80 μs and 7.68 ms was used to obtain buildup curves for the cross-peaks observed in the 2D spectrum. $^{1}H/^{1}H$ SQ−DQ experiments were performed utilizing a short back-to-back (BABA) cycle[28,37] to excite and convert the DQ signals. The excitation/reconversion time was set to 60 μs.

High-resolution solid-state ^{13}C and ^{15}N chemical shift NMR spectra and two-dimensional $^{1}H/^{13}C$ heteronuclear correlation (HETCOR) spectra for ABZ I and II were performed at room temperature on a Bruker Avance II spectrometer operating at a resonance frequency of 300.13 MHz for protons, 75.46 MHz for carbons, and 30.42 MHz for nitrogens, and equipped with a 4 mm MAS probe. The ^{13}C and ^{15}N chemical shift NMR spectra were recorded using the ramp-cross-polarization magic angle spinning (CPMAS) sequence[38,39] at 10 kHz MAS, utilizing the SPINAL64 pulse sequence for proton decoupling during acquisition.[40] Glycine was used as an external reference for ^{13}C chemical shifts and also for setting the Hartmann−Hahn matching condition in the CPMAS experiments.[41,42] The ^{15}N CPMAS spectra were referenced to solid glycine (δ = −347.6 ppm), and then the chemical shifts were converted to the nitromethane scale. ^{13}C spectra were recorded with 1600 scans, with a contact time of 1.5 ms and a recycle delay of 5 s. ^{15}N spectra were recorded with 6000 scans, a contact time of 5 ms, and a recycle delay of 5 s. Quaternary carbon and methyl group-only spectra were also recorded for ABZ I and II at 10 kHz MAS. Following the cross-polarization period, a delay of 40 μs was introduced prior to the acquisition period without applying any radiofrequency pulses on ^{1}H and ^{13}C channels, resulting in a rapid decay for the CH and CH_2 signals due to their strong $^{1}H-^{13}C$ dipolar couplings. The signals of CH and CH_2 groups can thus be suppressed, leaving only the signals of quaternary carbon and methyl group.[43] Protonated nitrogens (NH groups) were edited by recording CPMAS spectra of ABZ I and II, with a contact time of 1 ms.

Two-dimensional $^{1}H/^{13}C$ HETCOR spectra were recorded following the sequence presented by van Rossum et al.[44] The pulse sequence starts with a $(\pi/2 + \theta_m)$ pulse on protons, where θ_m is the magic angle, followed by a train of off-resonance frequency-switched Lee−Goldburg (FSLG) pulses[45,46] (or flip-flop LG (FFLG)[47]) to cancel the first two terms of the $^{1}H-^{1}H$ dipolar coupling Hamiltonian in the tilted rotating frame. FSLG irradiation was applied during the t_1 evolution period in successive times τ corresponding to a complete 2π rotation around the tilted axis. After the train of FSLG pulses, the proton magnetization is flipped back in the transverse plane by the magic-angle pulse. A ramped-amplitude CP sequence[31] was used to enhance ^{13}C signals, and the SPINAL64 pulse sequence[32] was used to decouple protons during ^{13}C signal acquisition. The period τ was set to 7.68 μs. The CP contact time was set to 200 μs to avoid any relayed homonuclear spin-diffusion-type processes, and the recycle delay was 5 s. The duration of the magic-angle pulse was 2.55 μs. Sixty-four t_1 increments with a dwell time of 35.5 μs, corresponding to a total acquisition time of 1.14 ms, were used. The spinning rate was 10 kHz.

3. RESULTS AND DISCUSSION

3.1. Characterization of ABZ Solid Forms. In this section, the properties of the two forms of ABZ are discussed, and the associated results pertaining to the various complementary techniques used (PXRD, DSC, TGA, solution NMR, and FT-IR) are analyzed to characterize and unequivocally distinguish the two solids.

Solution ^{1}H and ^{13}C NMR spectra were utilized to characterize the structures of ABZ I and II forms in the liquid state (see Supporting Information, Figure S3). Additionally, thermal analysis was used to distinguish both desmotropes of ABZ (see Supporting Information, Figure S6).

Figure 1 shows the experimental PXRD patterns for the two forms. In agreement with the previously reported results for form I,[48,49] our PXRD pattern shows several main peaks located at 6.9°, 11.3°, 11.6°, 13.8°, 17.9°, 18.8°, 19.9°, 22.1°, 24.4°, 24.7°, 27.2°, and 30° 2θ angles. However, diffraction peaks located at 7.3°, 10.7°, 12.4°, 14.6°, 18.1°, 24.7°, 25.6°, 29.5°, and 30.7° (2θ) are observed for the recrystallized ABZ, which are consistent with the results previously obtained by Pranzo et al. for form II.[9] Then, our PXRD results confirmed the phase purity of both solid forms.

The energetic changes related to tautomerism generate different electronic conditions that affect some vibrational states. These changes motivated us to perform studies on the IR spectra to evaluate the ABZ tautomerism. As shown in Figure 2, the FT-IR spectra of ABZ I and ABZ II revealed additional evidence to distinguish both tautomeric forms of ABZ. Table 1 displays the assignment of the bands. Both solid forms show characteristics bands at the same wavenumber for the NH stretching vibration, the carbonyl group of the

DOI: 10.1021/mp500539g
Mol. Pharmaceutics XXXX, XXX, XXX−XXX

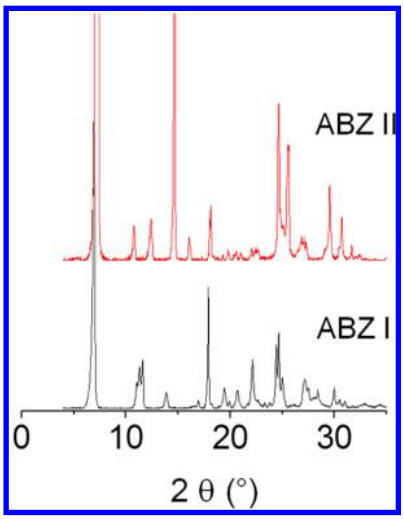

Figure 1. PXRD patterns for ABZ I and II.

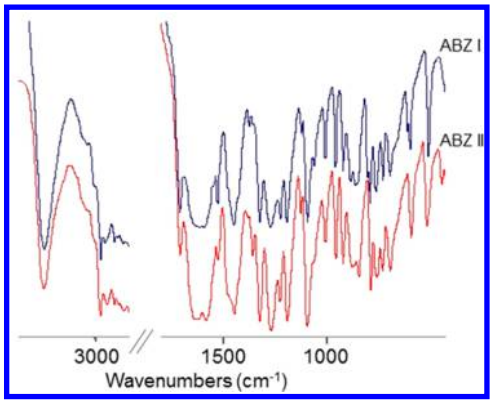

Figure 2. FT-IR spectra of ABZ I and ABZ II.

Table 1. FT-IR Absorption Bands

band assignment	wavenumber (cm^{-1})	
	ABZ I	ABZ II
NH stretching	3325	3325
carbonyl group	1708	1708
$-CH_3$ absorption	1443	1443
−CH stretching	2953, 2926	2957, 2912
C═N stretching	1654, 1591	1629, 1578
−CH deformation	1373	1377
fingerprint region	885, 863, 850, 805, 759, 728, 611, 597, 509	881, 866, 846, 767, 755, 732, 597, 588, 520, 447

carbamate moiety, and the $-CH_3$ absorption, while the bands corresponding to the −CH stretching vibration, the C═N stretching, and the −CH deformation appeared slightly shifted. These differences in the band positions evidenced that the C═N bond between the C2 and the N of carbamate in tautomer II of ABZ is energetically different to the corresponding bond between the C2 and the N of the heterocycle in ABZ I. In addition, the bands in the fingerprint region (between 1500 and 600 cm^{-1}) show marked differences between both solid forms, which can be used to identify and distinguish them. In particular, the spectrum of ABZ II shows shifted bands as well as new bands in comparison with that of ABZ I. ABZ I is characterized by bands at 885, 863, 850, 805, 759, 728, 611, 597, and 509 cm^{-1}, whereas ABZ II exhibits characteristic bands at 881, 866, 846, 767, 755, 732, 597, 588, 520, and 447 cm^{-1}. It is worth mentioning here that the bands observed for ABZ II revealing marked differences between both solid forms have not been previously reported.

3.2. Solid-State NMR Studies of Molecular Interactions. *3.2.1. Ultrafast MAS ^1H NMR Spectra.* Shown in Figure 3a are the 1D ^1H NMR spectra of ABZ forms I and II obtained at 50 kHz MAS at the same experimental conditions. Each ^1H spectrum shows five resolved peaks corresponding to the two NH protons, the aromatic protons (H6, H8, H9), the protons in the $O-CH_3$ group (H14), and the protons in the aliphatic chain (H16, H17, H18). Despite the apparent similarities of the two spectra, a closer inspection reveals that there is a nonsystematic shift for all the peaks to a lower ppm for form II compared to those for form I. In addition, if both spectra are compared some differences can be noted, especially those at around 6 ppm, with a shoulder in ABZ II that is absent in ABZ I. On the basis of previous assignments from ^1H solution NMR spectra (as also shown in Figure S3),[50,51] the signals for the non-nitrogen protons have been assigned. Table 2 reports chemical shift values for protons in both ABZ forms, where some values have been extracted directly from the $^1H/^1H$ SQ−DQ correlations, as in the case of aromatic protons, and from the $^1H/^{13}C$ HETCOR experiment for aliphatic chain protons. An important difference between the solid forms I and II is the assignment of the NH protons. Herein, these protons have been distinguished through 2D correlation spectra, namely, the $^1H/^1H$ SQ−SQ fp-RFDR at a short mixing time and $^1H/^1H$ SQ−DQ spectra, and confirmed by the $^1H/^{13}C$ HETCOR correlation experiments (see below). Taking into account the 2D HETCOR spectra (see below), the ^1H NMR signal at ∼14 ppm has been assigned to H10 in form I and to H1 in form II, where the signal at ∼11 ppm was assigned to H3. These results reveal that each solid form is present in a unique tautomeric form, which is in agreement with the possible tautomers of benzimidazole carbamates reported by Kassetti et al.[10]

T_1 values (around 3−5 s) measured for each peak in the ^1H NMR spectra of forms I and II show that the T_1 values for form I are slightly greater than their counterparts for form II, i.e., $T_1(I) > T_1(II)$ (see Table T1 in the Supporting Information).

3.2.2. ^{13}C CPMAS and 2D $^1H/^{13}C$ HETCOR. Figure 3b displays the ^{13}C CPMAS spectra for ABZ I and II. Tentative assignments have been performed taking into account the reported results for ABZ I in the solid state[52] and the nonquaternary suppression spectra that display quaternary carbons and methyl groups (see Figure S4 in the Supporting Information). It is obvious that the ^{13}C CPMAS spectra of ABZ I and ABZ II show differences, both in peak positions and peak splittings. For example, the peaks corresponding to C11 and C14 appear respectively at 160 and 53 ppm in form I, whereas they resonate at 162 and 52 ppm, respectively, in form II. Signals belonging to the group of C7, C9, C6 shifted and split in form I. In addition, peak splitting is observed for C16, C17, and C18 in the ABZ I spectrum, whereas only the C18 peak shows splitting in the case of ABZ II. These multiple peaks observed could be due to the presence of more than one conformation of the alkyl chain in the crystallographic asymmetric unit.

DOI: 10.1021/mp500539g
Mol. Pharmaceutics XXXX, XXX, XXX−XXX

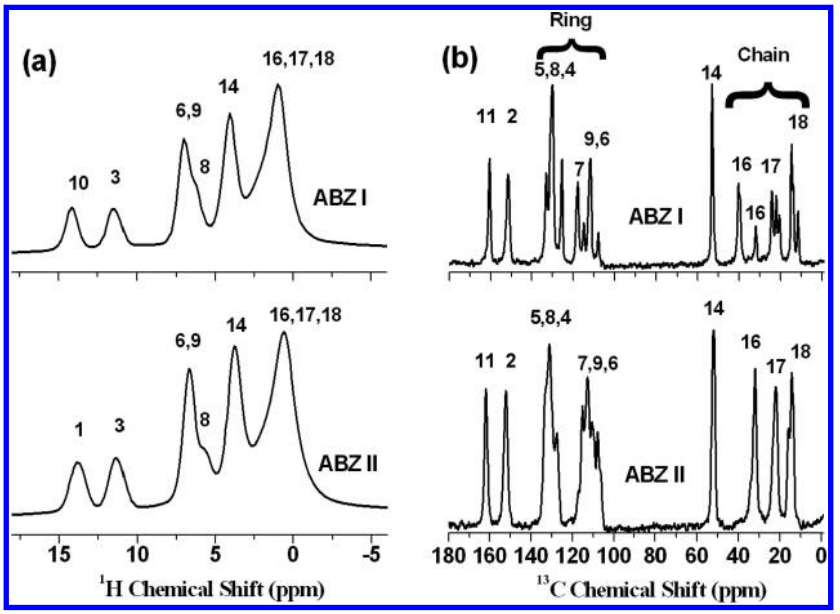

Figure 3. (a) ^{1}H NMR spectra obtained at 50 kHz MAS of ABZ I and II. (b) ^{13}C cross-polarization MAS spectra at 10 kHz MAS of ABZ I and II. Numbering of peaks in spectra corresponds to that in Scheme1.

Table 2. ^{1}H NMR Chemical Shifts (in ppm) Measured from ^{1}H Spectra Obtained at 50 kHz MAS; Some of the Chemical Shift Values Were Extracted Directly from the 2D ^{1}H/^{1}H SQ–DQ and/or ^{1}H/^{13}C HETCOR spectra

		chemical shifts (ppm)	
^{1}H	chemical group	I	II
H1 or H10	NH	14.2	13.8
H3	NH	11.5	11.3
H6, H9	ring	7.0	6.7
H8		6.1	5.7
H14	O–CH_3	4.1	3.7
H16, H17	chain-CH_2	1.2	1.1
H18	chain-CH_3	1.0	0.6

The 2D ^{1}H/^{13}C HETCOR MAS NMR spectra performed at 10 kHz MAS are shown in Figure 4 for ABZ I and II. A short contact time of 200 μs was used during the CP period that allows developing short-range heteronuclear correlations only. The ^{1}H projection in the indirect dimension shows a very similar feature to the 1D ^{1}H spectra under 50 kHz MAS (Figure 3a). The 2D spectra reveal well-resolved correlations between carbons and their neighboring protons. In particular, the well-resolved correlations displayed between carbon and protons in the aliphatic chain (16, 17, 18) enable the extraction of the NMR chemical shifts of the corresponding protons, which appear unresolved in the 1D ^{1}H spectra (see Table 2).

It is important to analyze and compare the correlations that exist between NH protons and their neighboring carbons in both forms I and II. In ABZ I, H3 correlates with the quaternary carbon C2, the quaternary C4 in aromatic ring, and the nonquaternary C9. The NH proton at around 14 ppm correlates with C11 and C2, and with the quaternary carbon C5. Thus, the proton at 14 ppm can be assigned to H10 in form I. In ABZ II, however, H3 correlates with C2 and C4, as expected. However, the NH proton at 14 ppm correlates with C2 but does not correlate with C11, which leads to the absence of C11 signal in the carbon projection (Figure 4b). Taking into

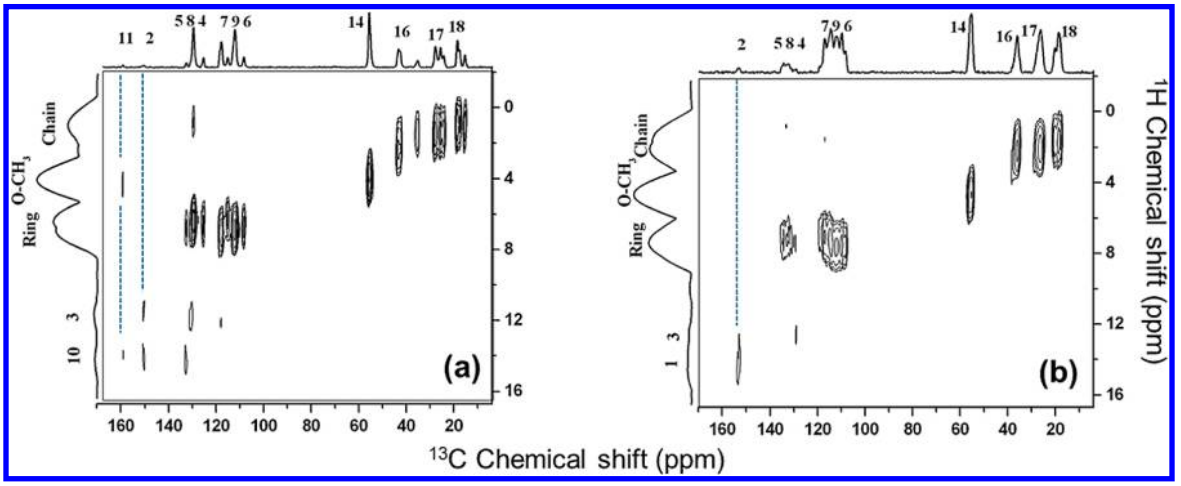

Figure 4. Two-dimensional ^{1}H/^{13}C HETCOR spectra of ABZ I (a) and ABZ II (b). ^{13}C and ^{1}H projections are displayed in the direct and indirect frequency dimensions, respectively. Some of the carbon–proton correlation peaks are marked with dashed lines.

DOI: 10.1021/mp500539g
Mol. Pharmaceutics XXXX, XXX, XXX–XXX

account that the 200 μs of contact time during CP will show only the stronger heteronuclear correlations in the HETCOR spectra, the NH group at 14 ppm in ABZ II can be assigned to H1. This fact provides unique information about the tautomers in ABZ, as shown in Scheme 1. Our proton assignments (performed by ssNMR) are in accordance with single crystal data available for ABZ II.[9] In addition, form I corresponds to tautomer C, and form II corresponds to tautomer B, which is proposed in the study of Kasetti et al. in ref 10, based on electronic structure analysis in similar compounds. Our results allow us to confirm the desmotropy of ABZ, which was previously classified as polymorphism.

3.2.3. ^{15}N CPMAS Spectra. ^{15}N spectra are useful to help in distinguishing desmotropes.[53] Figure 5 displays the ^{15}N CPMAS spectra for ABZ I and II. Assignments in each solid form have been performed taking into account edition spectra of protonated nitrogens, spectral assignments calculations,[54] and simulated chemical shifts. In the ^{15}N spectra of ABZ I and II we can clearly see three signals in each spectra in a range of 20−30 ppm, two of them corresponding to protonated nitrogens (see Figure S5 in the Supporting Information). Our assignments are consistent with the fact that N3 is a protonated nitrogen involved in the same hydrogen bond in both solid forms, then it appears at similar chemical shifts: −256.8 ppm in ABZ I and −257.8 ppm in ABZ II. However, N10 displays a shift from −228.4 in I to −248.8 ppm in II, and N1 displays a shift from −253.3 in I to −240.0 in II, revealing a marked difference in the protonated states in both solid forms. These shifts are also affected by the fact that N1 and N10 are involved in intermolecular hydrogen bonds (Scheme 2). Our results are consistent with the tautomeric differences between both solid forms observed by $^{1}H/^{13}C$ HETCOR spectra, in agreement with Scheme 1.

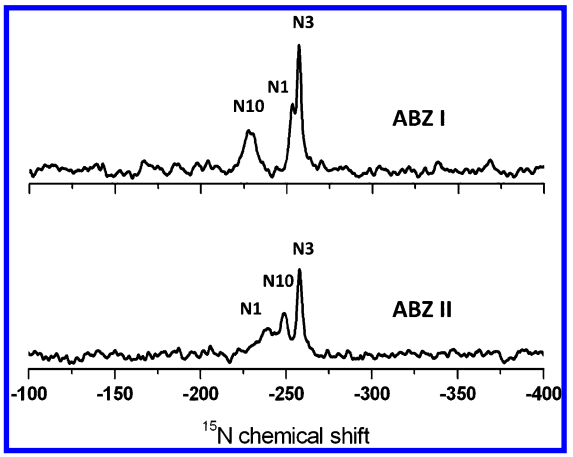

Figure 5. ^{15}N CPMAS spectra at 10 kHz MAS of ABZ I and II. Numbering of nitrogens corresponds to that in Scheme1

3.2.4. Two-Dimensional $^{1}H/^{1}H$ fp-RFDR Spectral Analysis. To observe proton−proton magnetization exchange mediated by proton−proton dipolar couplings, 2D $^{1}H/^{1}H$ fp-RFDR SQ−SQ experiments under 50 kHz MAS were performed. In the 2D fp-RFDR experiments,[26,27] the $^{1}H-^{1}H$ dipolar couplings, which are averaged out by the ultrafast MAS, are reintroduced by applying a series of rotor-synchronized 180° pulses during the mixing time.[23,25] Hence, the cross-peaks in the fp-RFDR spectrum originate from the combined effect of cross-relaxation (nuclear Overhausser effect, NOE) and spin diffusion through dipolar couplings (proportional to $1/r^3$ where r is the $^{1}H-^{1}H$ internuclear distance) among protons.[55,56]

Figure 6 shows the $^{1}H/^{1}H$ spectra of ABZ I and II obtained using the fp-RFDR pulse sequence for mixing times of 80 and 960 μs. The projection on each dimension corresponds to the ^{1}H spectra showing five peaks. Each peak corresponds to one proton in the case of H1, H10, H3, or protons with similar chemical shifts, as in the case of O−CH_3 group, the aromatic ring, and the aliphatic chain. The cross peak intensities at a given mixing time are related to the transfer of magnetization mediated by dipolar couplings between two protons that differ in their chemical shifts. At a short mixing time of 80 μs, both solid forms display small cross-peak intensities between a proton at ∼11 ppm (corresponding to NH) and protons at ∼4 ppm (assigned to group O−CH_3). At short mixing times, the emerging cross peaks appear due to the strong dipolar couplings, thus allowing for the identification and assignment of different protons. Then, the short mixing time correlation spectrum supports the assignment of the NH proton at ∼11 ppm as H3, giving further evidence of an intramolecular hydrogen bond involving N3−H3 and one oxygen atom, either O12 or O13. At 80 μs mixing time, the (ring, H14) correlation for both solid forms can be also observed, which implies the existence of an interaction between molecular fragments that are not in close spatial proximity in the same molecule. This cross-peak can be attributed to an intermolecular proximity, giving evidence to the existence of dimeric states, as shown in Scheme 2. Dimeric arrangements have been observed in ABZ II by single crystal X-ray diffraction[9] and have been proposed for similar compounds by quantum chemical calculations.[10] It is important to mention that although a single crystal structure is available for form II, our conclusions were extracted completely from a ssNMR point of view. In this study, direct observation of the dimeric conformations in both forms I and II of ABZ is made possible by virtue of the high resolution afforded by

Scheme 2. Dimeric Structures of Desmotropes (a) ABZ I and (b) ABZ II, Showing the Possible Intermolecular Interactions and Intramolecular Hydrogen Bonds

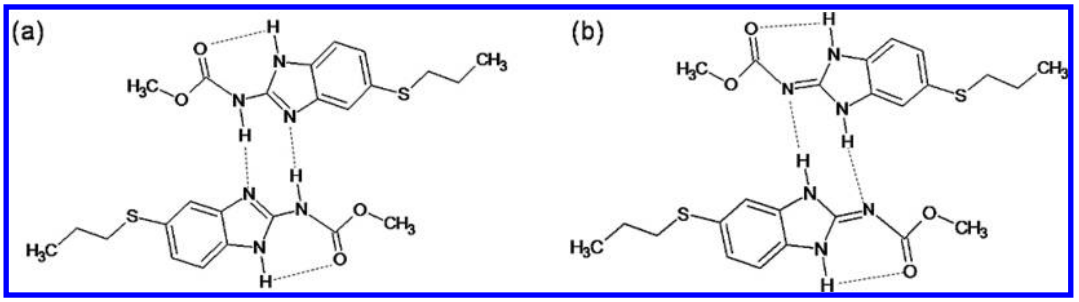

DOI: 10.1021/mp500539g
Mol. Pharmaceutics XXXX, XXX, XXX−XXX

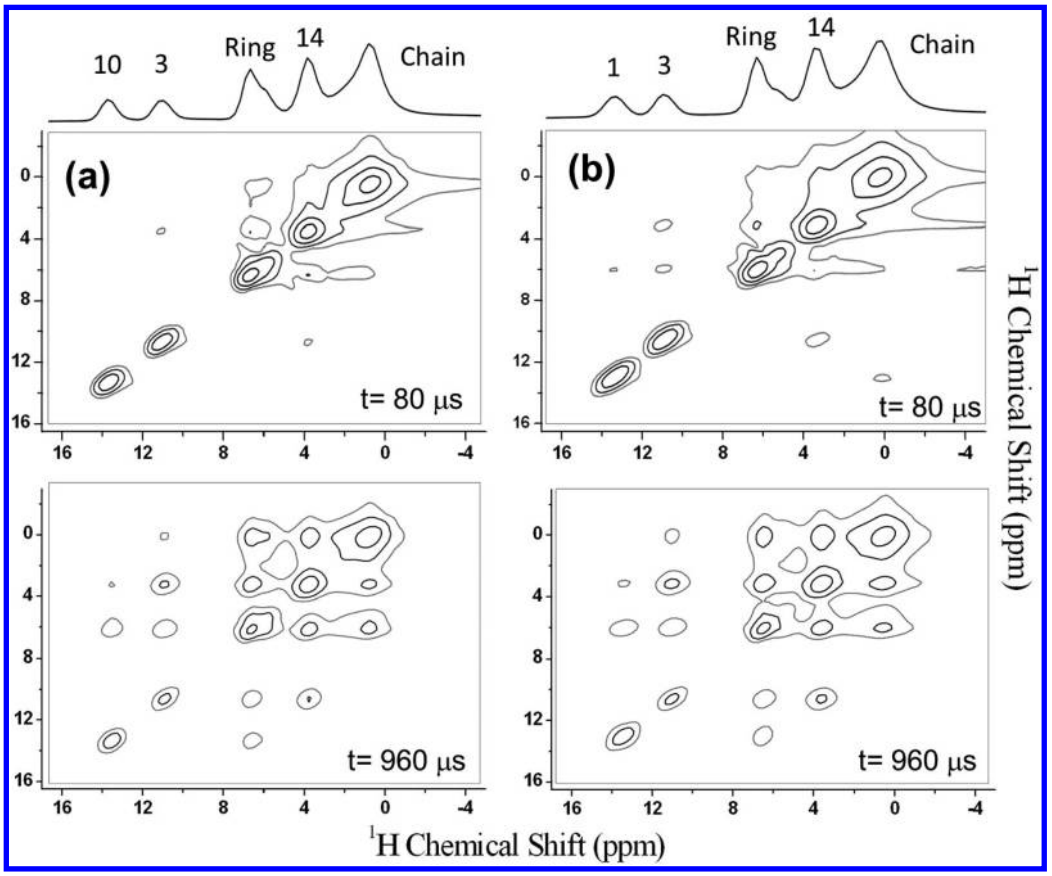

Figure 6. Two-dimensional ^{1}H/^{1}H fp-RFDR spectra of ABZ I (a) and ABZ II (b), corresponding to mixing times of 80 μs (top) and 960 μs (bottom), obtained at 50 kHz MAS. Projections for each 2D spectrum are displayed on both frequency axes.

ultrafast MAS. The dimers are characterized by intermolecular hydrogen bonds connecting N1 and N10. The dimeric arrangement enables for close proximity between the O−CH_3 group and the aromatic ring of molecules in the dimer, leading to an N3−H3···O12 hydrogen bond, as shown in Scheme 1. The strong (ring, chain) cross-peak is noticeable at short mixing times due to the proximity between these groups within the molecule. At a mixing time of 960 μs, all the cross-peaks are developed, as can be seen in Figure 6.

The intensity of the cross-peaks changes with the mixing time, having a build-up curve that reaches a maximum related to the proximity of the interacting protons and a global decay produced by the spin diffusion with a bath of spins. Assuming that the transfer of magnetization (and a given cross-peak) involves two peaks, then the cross-peak intensity between peak A and peak B, $I_{AB}(t)$, as a function of mixing time t, follows an equation of the form

$$I_{AB}(t) = I_0 \exp(-tR_1)(1 - \exp(-tR)) \quad (1)$$

where R is the build-up rate arising from longitudinal magnetization exchange between A and B, and R_1 is the overall relaxation rate produced by spin-diffusion with all the other protons in the sample as well as the T_1 relaxation. This equation describes the behavior of proton magnetization transfer in a two-spin system via dipolar couplings (e.g., cross-polarization),[13,39] and it is well-known for chemical exchange in a two-spin system.[57] To overcome possible imperfections in the recoupling π pulses during the fp-RFDR mixing period, we employed the XY4 phase cycling scheme, which has recently been proven to overcome such imperfections.[24] Figure 7 shows the experimental build-up curves for the cross-peaks in the 2D fp-RFDR experiments together with the fittings to eq 1 for ABZ I and II.

Table 3 shows the rate parameters extracted from the fittings for the cross-peak intensities measured for the peaks observed in the part above diagonal of the 2D spectra. Correlations corresponding to group of spins with closer proximity undergo faster transfer of magnetization, leading to larger build-up rate (R) values. Cross-peaks with build-up rate lower than 1 ms^{-1} are not displayed in the table. The results shown in Table 3 reveal that the fastest exchange of proton magnetization in both forms of ABZ occurs for the cross-peak (H3, H14). This observation provides further evidence on the presence of the intramolecular N3−H3···O12 hydrogen bond. In addition, a considerable exchange occurs between the aromatic protons and H3 due to their proximity in the molecule.

Both solid forms of ABZ exhibit fast magnetization exchange between H14 protons and the aromatic protons (3.5 ms^{-1} in I and 2.8 ms^{-1} in II), as well as a strong (H14, Chain) spatial connection with an exchange rate of around 2 ms^{-1}. These connections are due to the intermolecular dimeric arrangements in both solid forms of ABZ; these dimeric structures involve a hydrogen bond that connects N1 and N10. The cross-peak between NH proton at 14 ppm and the aromatic protons has a faster exchange rate in form I (2.4 ms^{-1}) than in form II (1.9 ms^{-1}). As these protons are involved in the intermolecular hydrogen bonds and display cross-peaks with aromatic rings, the difference in the exchange rate may indicate that different protons in each solid form are involved in hydrogen bonds, which is in accordance with tautomerism characteristic of this

DOI: 10.1021/mp500539g
Mol. Pharmaceutics XXXX, XXX, XXX−XXX

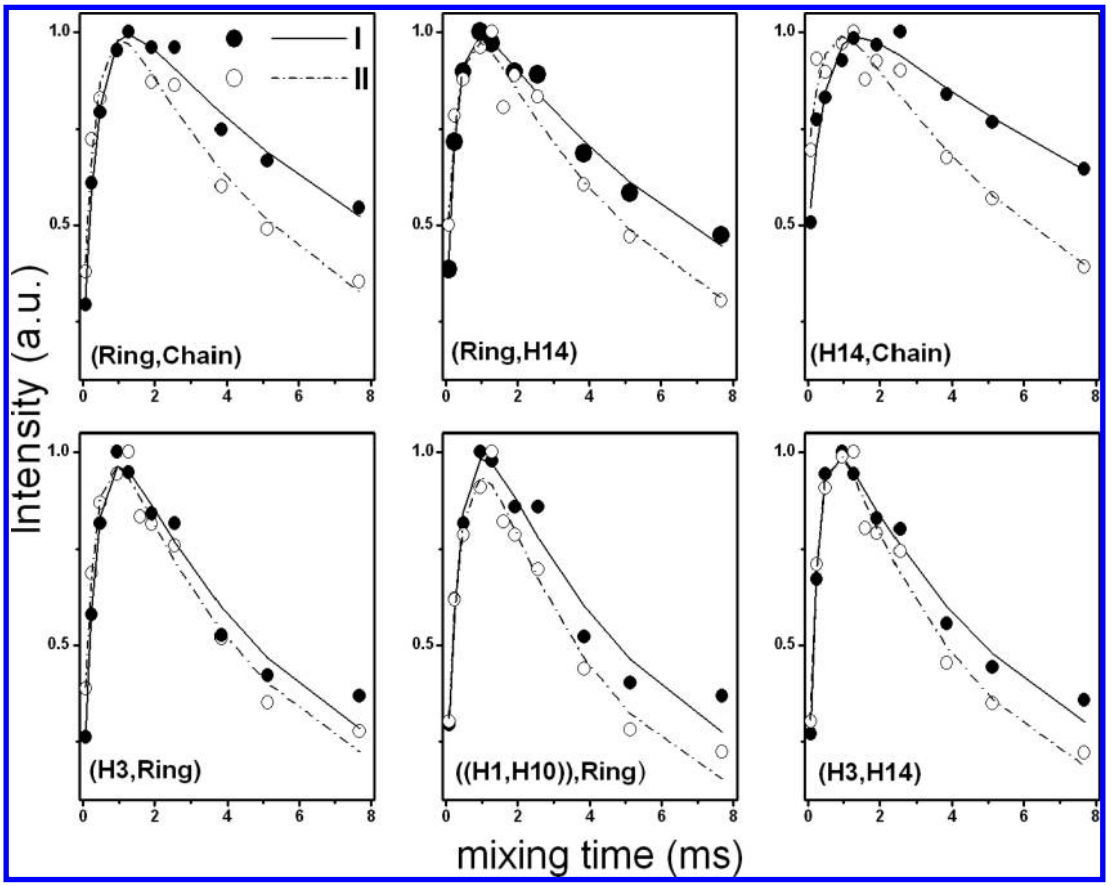

Figure 7. Normalized experimental build-up curves determined from the cross-peak intensities as a function of the mixing time in the 2D fp-RFDR experiment (black dots for form I and open circles for form II), together with the fittings obtained using eq 1 (solid lines for form I and dashed-dotted lines for form II) corresponding to the strongest correlations are displayed.

Table 3. Build-up (R) and Spin−Lattice Relaxation (R_1) Rates Obtained from the Fittings of Experimental Build-up of Intensity vs Mixing Time from eq 1 for the Cross-Peaks Observed in the 2D fp-RFDR Spectra of ABZ Desmotropes; Fitting Errors Are within 15% (for R) and 10% (for R_1)

	build-up rate R (ms^{-1})		relaxation rate R_1 (ms^{-1})	
cross-peak	I	II	I	II
(ring, chain)	2.3	2.5	0.10	0.17
(ring, H14)	3.5	2.8	0.12	0.17
(H14, chain)	2.0	2.1	0.10	0.14
(H3, ring)	2.7	2.7	0.20	0.22
((H1,H10), ring)	2.4	1.9	0.20	0.28
(H3, H14)	4.0	3.4	0.20	0.25

class of compounds.[10] A faster exchange involving the aromatic protons in form I can be attributed to the closer proximity between the atoms forming the N10−H10···N1 hydrogen bond in form I, as compared to those involved in the N1−H1···N10 bond in form II. In both solid forms there is a cross peak that involves protons in the ring and the chain, with a moderate exchange rate due to their proximity within the molecule. In agreement with the trend followed by the spin−lattice relaxation times (T_1) discussed earlier, the results in Table 3 show that proton relaxation rates are slightly faster in form I than in form II [i.e., $R_1(\mathrm{I}) < R_1(\mathrm{II})$].

3.2.5. Two-Dimensional $^1H/^1H$ SQ−DQ Spectral Analysis. Figure 8 shows the $^1H/^1H$ SQ−DQ spectra for ABZ I and II, and the extracted correlations are listed in Table 4. In the DQ dimension, correlations are located at the sum of chemical shift frequencies of the two nuclei involved. Peaks on the diagonal are due to dipolar couplings between protons with similar chemical shifts, whereas other correlation peaks appear symmetric with respect to this diagonal. In general, the presence of a correlation peak in a DQ solid-state NMR spectrum of an organic solid recorded with very short DQ excitation time indicates a spatial $^1H-^1H$ separation of less than 3 Å.[29]

The $^1H/^1H$ SQ−DQ spectra show strong autocorrelation for the protons in the aliphatic chains of both ABZ I and II, at 1.9 and 1.3 ppm in the DQ dimension, respectively. In both solid forms, a strong autocorrelation exists between the three H14 protons at 8.0 and 7.3 ppm. However, there are noticeable autocorrelations at 28.4 ppm in form I and 28.0 ppm in form II, in the DQ dimension. These autocorrelations correspond to protons at 14 ppm. As these are single protons in the molecule, an autocorrelation gives evidence of proximity between two separate molecules. The mentioned H10−H10 correlation in form I and H1−H1 correlation in form II are in accordance with the proximity between the hydrogen bonds connecting the tautomers in their dimeric state: N10−H10···N1 in form I and N1−H1··· N10 in form II (see Scheme 2). These hydrogen bonds also explain the presence of correlations between the NH protons and the aromatic ring protons at 21.7 and 20.7 ppm in forms I and II, respectively.

The presence of the H3−H14 correlation is a strong evidence of the intramolecular N3−H3···O12 hydrogen bond. The H3−H9 correlations present in forms I and II enable the

DOI: 10.1021/mp500539g
Mol. Pharmaceutics XXXX, XXX, XXX−XXX

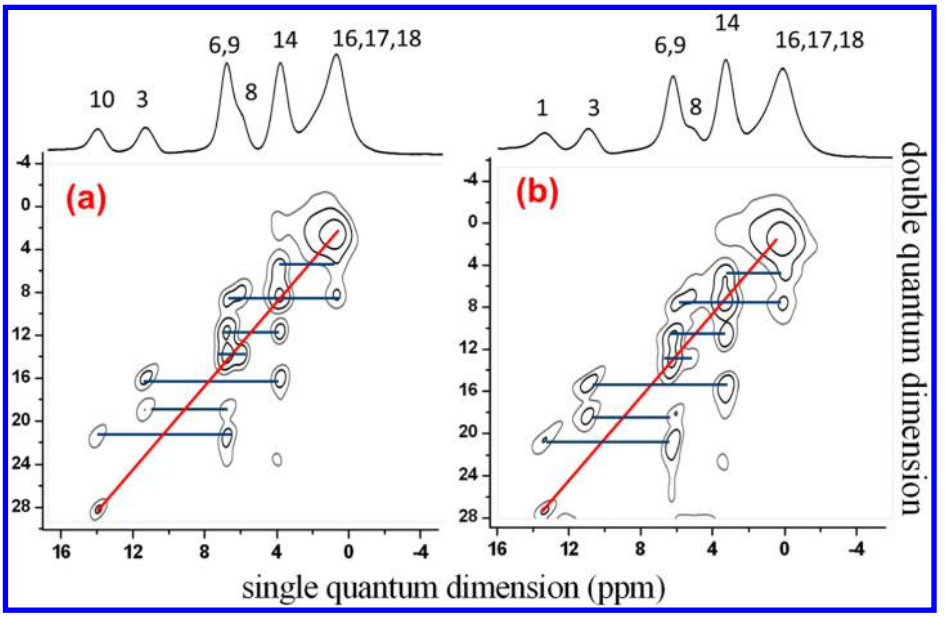

Figure 8. Two-dimensional $^{1}H/^{1}H$ SQ–DQ solid-state NMR spectra of ABZ I (a) and ABZ II (b) obtained at 50 kHz MAS. One-dimensional ^{1}H spectra are displayed in the direct dimension (top). Correlations in the double quantum dimension are marked with a line joining the correlated peaks. The peaks on the diagonal arise from autocorrelations.

Table 4. Correlations in the DQ Dimension of the 2D $^{1}H/^{1}H$ SQ–DQ Solid-State NMR Spectra Obtained from ABZ I and II Samples

correlation	$\omega_a + \omega_b$ (ppm) ABZ I	correlation	$\omega_a + \omega_b$ (ppm) ABZ II
H10–H10	28.4	H1–H1	28.0
H10 – H6	21.7	H1–H6	20.7
H3–H9	19.3	H3–H9	18.7
H3–H14	15.9	H3–H14	15.7
H6–H9	13.8	H6–H9	12.7
H6,9–H8	13.5	H6,9–H8	12.7
H6–H14	11.3	H6–H14	10.6
H6,9–H16,17	8	H6,9–H16,17	7.3
H8–H16,H17	7.0	H8–H16,H17	6.8
H14–H14	8.0	H14–H14	7.3
H14–H16,H17	5.4	H14–H16,H17	5.2
H16,17,18–H16,17,19	1.9	H16,17,18–H16,17,19	1.3

assignment of H9 in both compounds. Correlations between protons in the aromatic rings are observed at 13.8 and 13.5 ppm in ABZ I and at 12.7 ppm in ABZ II. Correlations between the aromatic ring protons and the aliphatic chain protons are clearly displayed at 8.0 and 7.0 ppm in form I and at 7.3 and 6.8 ppm in form II. There is also an important correlation between H6 and H14, which is supported by the dimeric arrangement in both compounds. Correlation peaks observed at 21.5 ppm for form I and 21.9 ppm for form II allow the assignment and identification of H6. H14 protons are involved in correlation with chain protons, which are relatively far within the molecule, appearing at 5.4 ppm in I and at 5.2 ppm in II. These correlations are of low intensity and are probably due to the dimeric structure.

4. CONCLUSIONS

The results obtained in this study proved the desmotropy of the two solids forms of ABZ, I and II. High-resolution 2D ssNMR results rendered detailed information about the hydrogen bonding and the dimeric arrangements in both desmotropes of ABZ. Intramolecular and intermolecular interactions were directly observed by the conjunction of ^{1}H-detected ultrafast MAS ssNMR experiments, such as $^{1}H/^{1}H$ SQ–SQ fp-RFDR and $^{1}H/^{1}H$ SQ–DQ spectra. In particular, each tautomer was unambiguously identified from the $^{1}H/^{13}C$ HETCOR spectra, where form I corresponds to the tautomer C, while form II corresponds to the tautomer B, as proposed in a recent study by Kasetti et al.[10] ^{15}N solid state spectra confirmed our conclusions of different tautomeric states for ABZ I and II. It is worth noting that, although tautomer C of ABZ II and its dimeric arrangement have been previously reported by single crystal X-ray diffraction,[9] no such information on the solid-state molecular arrangement of solid form I is available in the literature. Moreover, an important intramolecular hydrogen bond that has a potential influence on the solubility of ABZ has been clearly characterized and discussed in the present study. Indeed, the great similarity in 1D ^{1}H spectra and 2D $^{1}H/^{1}H$ spectra in ABZ I and II may indicate that the differences in the solid forms only rely on the mentioned tautomeric and dimeric states, making ^{1}H NMR MAS techniques less sensitive to distinguish desmotropes. However, NMR experiments that involve ^{13}C and ^{15}N are more reliable to distinguish and characterize desmotropes and different solid forms.

In summary, the results presented in this study constitute the first report about ABZ desmotropy explored by solid-state NMR spectroscopy.

■ ASSOCIATED CONTENT

Ⓢ Supporting Information

NMR and thermal analysis. This material is available free of charge via the Internet at http://pubs.acs.org.

■ AUTHOR INFORMATION

Corresponding Authors

*E-mail: chattah@famaf.unc.edu.ar.
*E-mail: claudiagarnero@gmail.com.

DOI: 10.1021/mp500539g
Mol. Pharmaceutics XXXX, XXX, XXX–XXX

Notes

The authors declare no competing financial interest.

■ ACKNOWLEDGMENTS

The authors thank Professor Adam Matzger from the University of Michigan for PXRD results and thermal analysis experiments. Solid-state NMR studies carried out at the University of Michigan are supported by the funds from the National Institutes of Health (GM084018 and GM095640 to A.R.). We are grateful for financial support from the Consejo Nacional de Investigaciones Científicas y Técnicas (CONICET), the Secretaria de Ciencia y Técnica de la Universidad Nacional de Córdoba (SECyT-UNC), and Ministerio de Ciencia y Tecnología (MinCyT) de la Provincia de Córdoba. A.K.C. thanks the Universidad Nacional de Córdoba (UNC) for the support through the "Programa Cuarto Centenario para Profesores", which enabled the visit to the University of Michigan.

■ REFERENCES

(1) *Polymorphism: In the Pharmaceutical Industry*; Wiley-VCH: Berlin, Germany, 2006.

(2) Brittain, H. G. *Characterization of Pharmaceutical Compounds in the Solid State*; Academic Press: New York, 2011; Vol. *10*.

(3) Cook, G. C. Use of benzimidazole chemotherapy in human helminthiasis: indications and efficacy. *Parasitol. Today* **1990**, *6*, 133−136.

(4) Evrard, B.; Chiap, P.; DeTullio, P.; Ghalmi, F.; Piel, G.; Van Hees, T.; Crommen, J.; Losson, B.; Delattre, L. Oral bioavailability in sheep of albendazole from a suspension and from a solution containing hydroxypropyl-beta-cyclodextrin. *J. Controlled Release* **2002**, *85*, 45−50.

(5) World Health Organization. WHO Model List of Essential Medicines, 18th List, 2013. http://www.who.int/medicines/publications/essentialmedicines/18th_EML_Final_web_8Jul13.pdf.

(6) Critchley, J.; Addiss, D.; Gamble, C.; Garner, P.; Gelband, H.; Ejere, H. Albendazole for lymphatic filariasis. *Cochrane Database Syst. Rev.* **2005**, *4*, CD003753.

(7) Lloyd, A. E.; Honey, B. L.; John, B. M.; Condren, M. Treatment options and considerations for intestinal helminthic infections treatment options and considerations for intestinal helminthic infections. *J. Pharm. Technol.* **2014**, *30*, 130−139.

(8) Chassaing, C.; Berger, M.; Heckeroth, A.; Ilg, T.; Jaeger, M.; Kern, C.; Schmid, K.; Uphoff, M. Highly water-soluble prodrugs of anthelmintic benzimidazole carbamates: Synthesis, pharmacodynamics, and pharmacokinetics. *J. Med. Chem.* **2008**, *51*, 1111−1114.

(9) Pranzo, M. B.; Cruickshank, D.; Coruzzi, M.; Caira, M. R.; Bettini, R. Enantiotropically related albendazole polymorphs. *J. Pharm. Sci.* **2010**, 3731−3742.

(10) Kasetti, Y.; Bharatam, P. V. Tautomerism in drugs with benzimidazole carbamate moiety: An electronic structure analysis. *Theor. Chem. Acc.* **2012**, *131*, 1160−1168.

(11) Sundriyal, S.; Khanna, S.; Saha, R.; Bharatam, P. V. Metformin and glitazones: does similarity in biomolecular mechanism originate from tautomerism in these drugs? *J. Phys. Org. Chem.* **2008**, *21*, 30−33.

(12) Lindenberg, M.; Kopp, S.; Dressman, J. B. Classification of orally administered drugs on the World Health Organization Model List of Essential Medicines according to the biopharmaceutics classification system. *Eur. J. Pharm. Biopharm.* **2004**, *58*, 265−278.

(13) Geppi, M.; Mollica, G.; Borsacchi, S.; Veracini, C. A. Solid-state NMR studies of pharmaceutical systems. *Appl. Spectrosc. Rev.* **2008**, *43*, 202−302.

(14) Monti, G. A.; Chattah, A. K.; Garro Linck, Y. Solid-state nuclear magnetic resonance in pharmaceutical compounds. *Annu. Rep. NMR Spectrosc.* **2014**, *83*, 221−269.

(15) Linser, R.; Dasari, M.; Hiller, M.; Higman, V.; Fink, U.; Lopez del Amo, J.-M.; Markovic, S.; Handel, L.; Kessler, B.; Schmieder, P.; Oesterhelt, D.; Oschkinat, H.; Reif, B. Proton-detected solid-state NMR spectroscopy of fibrillar and membrane proteins. *Angew. Chem., Int. Ed.* **2011**, *50*, 4508−4512.

(16) Brown, S. P. Applications of high-resolution ^{1}H solid-state NMR. *Solid State Nucl. Magn. Reson.* **2012**, *41*, 1−27.

(17) Watt, E. D.; Rienstra, C. M. Recent advances in solid-state nuclear magnetic resonance techniques to quantify biomolecular dynamics. *Anal. Chem.* **2013**, *86*, 58−64.

(18) Tang, M.; Comellas, G.; Rienstra, C. M. Advanced solid-state NMR approaches for structure determination of membrane proteins and amyloid fibrils. *Acc. Chem. Res.* **2013**, *46*, 2080−2088.

(19) Asami, S.; Reif, B. Proton-detected solid-state NMR spectroscopy at aliphatic sites: Application to crystalline systems. *Acc. Chem. Res.* **2013**, *46*, 2089−2097.

(20) Nishiyama, Y.; Malon, M.; Ishii, Y.; Ramamoorthy, A. 3D ^{15}N/^{15}N/^{1}H chemical shift correlation experiment utilizing an RFDR-based ^{1}H/^{1}H mixing period at 100 kHz MAS. *J. Magn. Reson.* **2014**, *244*, 1−5.

(21) Baias, M.; Widdifield, C. M.; Dumez, J.-N.; Thompson, H. P. G.; Cooper, T. G.; Salager, E.; Bassil, S.; Stein, R. S.; Lesage, A.; Day, G. M.; Emsley, L. Powder crystallography of pharmaceutical materials by combined crystal structure prediction and solid-state ^{1}H NMR spectroscopy. *Phys. Chem. Chem. Phys.* **2013**, *15*, 8069−8080.

(22) Baias, M.; Dumez, J.-N.; Svensson, P. H.; Schantz, S.; Day, G. M.; Emsley, L. De novo determination of the crystal structure of a large drug molecule by crystal structure prediction-based powder NMR crystallography. *J. Am. Chem. Soc.* **2013**, *135*, 17501−17507.

(23) Ramamoorthy, A.; Xu, J. 2D 1H/1H RFDR and NOESY NMR experiments on a membrane-bound antimicrobial peptide under magic angle spinning. *J. Phys. Chem. B* **2013**, *117*, 6693−7000.

(24) Nishiyama, Y.; Zhang, R.; Ramamoorthy, A. Finite-pulse radio frequency driven recoupling with phase cycling for 2D 1H/1H correlation at ultrafast MAS frequencies. *J. Magn. Reson.* **2014**, *243*, 25−32.

(25) Ye, Y. Q.; Malon, M.; Martineau, C.; Taulelle, F.; Nishiyama, Y. Rapid measurement of multidimensional 1H solid-state NMR spectra at ultra-fast MAS frequencies. *J. Magn. Reson.* **2014**, *239*, 75−80.

(26) Bennett, A. E.; Rienstra, C. M.; Griffiths, J. M.; Zhen, W.; Lansbury, P. T.; Griffin, R. G. Homonuclear radio frequency-driven recoupling in rotating solids. *J. Chem. Phys.* **1998**, *108*, 9463−9479.

(27) Bennett, A. E.; Griffin, R. G.; Ok, J. H.; Vega, S. Chemical shift correlation spectroscopy in rotating solids: Radio frequency-driven dipolar recoupling and longitudinal exchange. *J. Chem. Phys.* **1992**, *96*, 8624−8627.

(28) Sommer, W.; Gottwald, J.; Demco, D. E.; Spiess, H. W. Dipolar heteronuclear multiple-quantum NMR spectroscopy in rotating solids. *J. Magn. Reson., Ser. A* **1995**, *113*, 131−134.

(29) Brown, S. P.; Spiess, H. W. Advanced solid-state NMR methods for the elucidation of structure and dynamics of molecular, macromolecular, and supramolecular systems. *Chem. Rev.* **2001**, *101*, 4125−4155.

(30) Gottwald, J.; Demco, D. E.; Graf, R.; Spiess, H. W. High-resolution double-quantum NMR spectroscopy of homonuclear spin pairs and proton connectivities in solids. *Chem. Phys. Lett.* **1995**, *243*, 314−323.

(31) Graf, R.; Heuer, A.; Spiess, H. W. Chain-order effects in polymer melts probed by H1 double-quantum NMR spectroscopy. *Phys. Rev. Lett.* **1998**, *80*, 5738.

(32) Brown, S. P.; Lesage, A.; Elena-Herrmann, B.; Emsley, L. Probing proton-proton proximities in the solid state: High-resolution two-dimensional ^{1}H-^{1}H double-quantum CRAMPS NMR spectroscopy. *J. Am. Chem. Soc.* **2004**, *126*, 13230−13231.

(33) Brown, S. P. Probing proton-proton proximieties in the solid State. *Prog. Nucl. Magn. Spectrosc.* **2007**, *50*, 199−251.

(34) Garro Linck, Y.; Chattah, A. K.; Graf, R.; Romañuk, C. B.; Olivera, M. E.; Manzo, R. H.; Monti, G. A.; Spiess, H. W. Multinuclear solid state NMR investigation of two polymorphic forms of ciprofloxacin-saccharinate. *Phys. Chem. Chem. Phys.* **2011**, *13*, 6590−6596.

DOI: 10.1021/mp500539g
Mol. Pharmaceutics XXXX, XXX, XXX−XXX

(35) Brown, S. P. Recent advances in solid-state MAS NMR methodology for probing structure and dynamics in polymeric and supramolecular systems. *Macromol. Rapid Commun.* **2009**, *30*, 688−716.
(36) Elguero, J. Polymorphism and desmotropy in heterocyclic crystal structures. *Cryst. Growth Des.* **2011**, *11*, 4731−4738.
(37) Feike, M.; Demco, D. E.; Graf, R.; Gottwald, J.; Hafner, S.; Spiess, H. W. Broadband multiple-quantum NMR spectroscopy. *J. Magn. Reson., Ser. A* **1996**, *122*, 214−221.
(38) Metz, G.; Wu, X. L.; Smith, S. O. Ramped-amplitude cross polarization in magic-angle-spinning NMR. *J. Magn. Reson., Ser. A* **1994**, *110*, 219−227.
(39) Harris, R. K. *Nuclear Magnetic Resonance Spectroscopy: A Physicochemical View*; Longman Scientific & Technical: Essex, U.K., 1986.
(40) Fung, B. M.; Khitrin, A. K.; Ermolaev, K. An improved broadband decoupling sequence for liquid crystals and solids. *J. Magn. Reson.* **2000**, *142*, 97−101.
(41) Schaefer, J.; Stejskal, E. O. Carbon-13 nuclear magnetic resonance of polymers spinning at the magic angle. *J. Am. Chem. Soc.* **1976**, *98*, 1031−1032.
(42) Pines, A.; Gibby, M. G.; Waugh, J. S. Proton-enhanced nuclear induction spectroscopy. A method for high resolution NMR of dilute spins in solids. *J. Chem. Phys.* **1972**, *56*, 1776.
(43) Opella, S. J.; Frey, M. H. Selection of nonprotonated carbon resonances in solid-state nuclear magnetic resonance. *J. Am. Chem. Soc.* **1979**, *101*, 5854−5856.
(44) van Rossum, B. J.; Förster, H.; de Groot, H. J. M. High-field and high-speed CP-MAS 13C NMR heteronuclear dipolar-correlation spectroscopy of solids with frequency-switched Lee−Goldburg homonuclear decoupling high-field and high-speed CP-MAS 13C NMR heteronuclear dipolar-correlation spectroscopy of solids with frequency-switched Lee−Goldburg homonuclear decoupling. *J. Magn. Reson.* **1997**, *124*, 516−519.
(45) Lee, M.; Goldburg, W. I. Nuclear magnetic resonance line narrowing by a rotating rf field. *Phys. Rev.* **1965**, *140*, A1261.
(46) Bielecki, A.; K, A. C.; Levitt, M. H. Frequency-switched pulse sequences: Homonuclear decoupling and dilute spin NMR in solids. *Chem. Phys. Lett.* **1989**, *155*, 341−346.
(47) Mehring, M.; Waugh, J. S. Magic-angle NMR experiments in solids. *Phys. Rev. B* **1972**, *5*, 3459.
(48) Alanazi, F. K.; El-Badry, M.; Ahmed, M. O.; Alsarra, I. A. Improvement of albendazole dissolution by preparing microparticles using spray-drying technique. *Sci. Pharm.* **2007**, *75*, 63−79.
(49) Saleh, N. i.; Khaleel, A.; Al-Dmour, H.; al-Hindawi, B.; Yakushenko, E. Host−guest complexes of cucurbit[7]uril with albendazole in solid state. *J. Therm. Anal. Calorim.* **2013**, *111*, 385−392.
(50) Ganesh, K.; Balraj, C.; Satheshkumar, A.; Elango, K. P. Spectroscopic investigation on the mechanism of formation of molecular complexes of albendazole and trimethoprim with 2, 3-dichloro-5, 6-dicyano-1, 4-benzoquinone. *Spectrochim. Acta, Part A* **2012**, *92*, 46−55.
(51) Cavalcanti, N. C. T.; Sousa, G. D.; Tabosa, M. A. M.; Soares Sobrinho, J. L.; Leal, L. B.; Santana, D. P. d. Assay and physicochemical characterization of the antiparasitic albendazole. *Braz. J. Pharm. Sci.* **2012**, *48*, 281−290.
(52) Paulekuhn, G. S.; Dressman, J. B.; Saal, C. Salt screening and characterization for poorly soluble, weak basic compounds: case study albendazole. *Pharmazie* **2013**, *68*, 555−564.
(53) Bauer, M.; Harris, R. K.; Rao, R. C.; Apperley, D. C.; Rodger, C. A. NMR study of desmotropy in irbesartan, a tetrazole-containing pharmaceutical compound. *J. Chem. Soc., Perkin Trans.* **1998**, *2*, 475−481.
(54) Blanco, F.; Alkorta, I.; Elguero, J. Statistical analysis of 13C and 15N NMR chemical shifts from GIAO/B3LYP/6-311++ G** calculated absolute shieldings. *Magn. Reson. Chem.* **2007**, *45*, 797−800.
(55) Higashi, K.; Yamamoto, K.; Pandey, M. K.; Mroue, K. H.; Moribe, K.; Yamamoto, K.; Ramamoorthy, A. Insights into atomic-level interaction between mefenamic acid and Eudragit EPO in a supersaturated solution by high-resolution magic-angle spinning NMR spectroscopy. *Mol. Pharmaceutics* **2014**, *11*, 351−357.
(56) Pandey, M. K.; Vivekanandan, S.; Yamamoto, K.; Im, S.; Waskell, L.; Ramamoorthy, A. Proton-detected 2D radio frequency driven recoupling solid-state NMR studies on micelle-associated cytochrome-b5. *J. Magn. Reson.* **2014**, *242*, 169−179.
(57) Bain, A. D. Chemical exchange in NMR. *Prog. Nucl. Magn. Reson. Spectrosc.* **2003**, *43*, 63−103.

DOI: 10.1021/mp500539g
Mol. Pharmaceutics XXXX, XXX, XXX−XXX